

Structure and mechanical properties of faults in the North Anatolian Fault system from InSAR observations of coseismic deformation due to the 1999 Izmit (Turkey) earthquake

Yariv Hamiel^{1,2} and Yuri Fialko¹

Received 29 September 2006; revised 28 February 2007; accepted 12 March 2007; published 19 July 2007.

[1] We study the structure and mechanical properties of faults in the North Anatolian Fault system by observing near-fault deformation induced by the 1999 M_w 7.4 Izmit earthquake (Turkey). We use interferometric Synthetic Aperture Radar (InSAR) and Global Positioning System observations to analyze the coseismic surface deformation in the near field of the Izmit rupture. The overall observed coseismic deformation is consistent with deformation predicted by a dislocation model assuming a uniform elastic crust. Previous InSAR studies revealed small-scale changes in the radar range across the nearby faults of the North Anatolian fault system (in particular, the Mudurnu Valley and Iznik faults) (e.g., Wright et al., 2001). We demonstrate that these anomalous range changes are consistent with an elastic response of compliant fault zones to the stress perturbation induced by the Izmit earthquake. We examine the spatial variations and mechanical properties of fault zones around the Mudurnu Valley and Iznik faults using three-dimensional finite element models. In these models, we include compliant fault zones having various geometries and elastic properties and apply stress changes deduced from a kinematic slip model of the Izmit earthquake. The best fitting models suggest that the inferred fault zones have a characteristic width of a few kilometers, depth in excess of 10 km, and reductions in the effective shear modulus of about a factor of 3 compared to the surrounding rocks. The characteristic width of the best fitting fault zone models is consistent with field observations along the North Anatolian Fault system (Ambraseys, 1970). Our results are also in agreement with InSAR observations of small-scale deformation on faults in the Eastern California Shear Zone in response to the 1992 Landers and 1999 Hector Mine earthquakes (Fialko et al., 2002; Fialko, 2004). The inferred compliant fault zones likely represent intense damage and may be quite commonly associated with large crustal faults.

Citation: Hamiel, Y., and Y. Fialko (2007), Structure and mechanical properties of faults in the North Anatolian Fault system from InSAR observations of coseismic deformation due to the 1999 Izmit (Turkey) earthquake, *J. Geophys. Res.*, 112, B07412, doi:10.1029/2006JB004777.

1. Introduction

[2] Faults in the Earth crust are often surrounded by finite zones of highly fractured rock (e.g., see a review by *Ben-Zion and Sammis* [2003]). Laboratory experiments and theoretical studies indicate that the degree of fracturing of the host rocks can be related to a reduction in the effective elastic moduli [e.g., *Hadley*, 1976; *Budiansky and O'Connell*, 1976; *Alm et al.*, 1985; *Pestman and Munster*, 1996; *Lyakhovskiy et al.*, 1997; *Hamiel et al.*, 2004; *Katz and Reches*, 2004; *Hamiel et al.*, 2006]. In principle, the difference between the elastic moduli of the fault zone and the surrounding rock should be

detectable through seismologic and geodetic observations. Recently, surface deformation anomalies have been detected on faults in the Eastern California Shear Zone (ECSZ) using interferometric Synthetic Aperture Radar (InSAR) observations of coseismic deformation induced by the 1992 M_w 7.3 Landers and 1999 M_w 7.1 Hector Mine earthquakes [*Fialko et al.*, 2002; *Fialko*, 2004]. These deformation anomalies were interpreted in terms of an elastic response of compliant fault zones to changes in the stress field induced by nearby earthquakes. The data suggest a contrast between the elastic moduli of the fault zone and the surrounding rock of about a factor of 2, and the width of low rigidity zones of 1–2 km. In this paper, we present results of a study of the mechanical properties of faults in the North Anatolian Fault system using observations of coseismic deformation due to the 17 August 1999, Izmit earthquake (Turkey).

[3] The North Anatolian Fault (NAF) is the largest and currently most active fault system in Turkey. It is approximately 1500 km long, extending from the northern part of

¹Institute of Geophysics and Planetary Physics, Scripps Institution of Oceanography, University of California, San Diego, La Jolla, California, USA.

²Now at Geological Survey of Israel, Jerusalem, Israel.

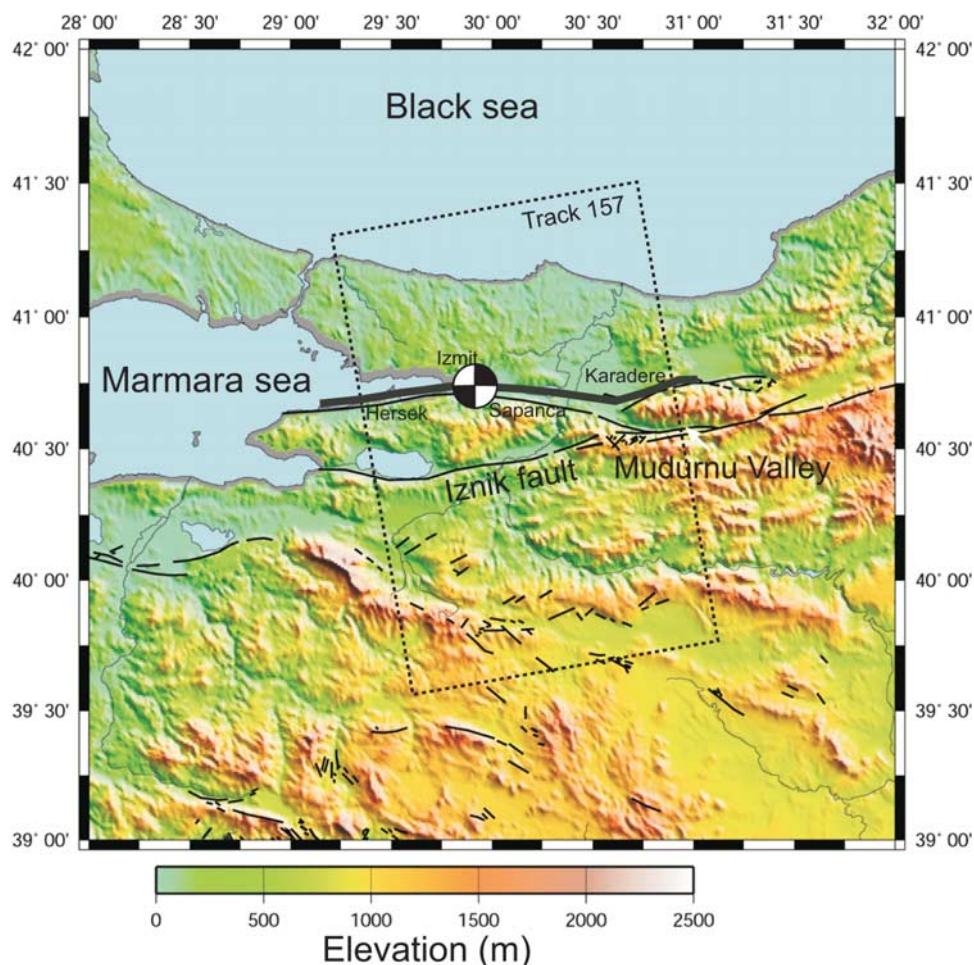


Figure 1. Topographic and tectonic map of the Izmit area. The “beach ball” indicates the location of the epicenter and focal mechanism of the Izmit earthquake. The thick black line represents the ruptured segments during the Izmit earthquake. Other faults in the area are shown by thin black lines. The dotted box outlines the ERS radar scene for the ascending orbit (track 157) used in this study.

the Aegean Sea to Karliova triple junction (Eurasia-Anatolia-Arabia) in Eastern Turkey, where it intersects with the East Anatolian Fault. The NAF defines the northern boundary of the Anatolian plate and accommodates the relative right-lateral motion between the Eurasian and Anatolian plates [e.g., Sengör *et al.*, 1985; Armijo *et al.*, 1999]. The 17 August 1999, Izmit earthquake (M_w 7.4 from long-period seismic wave data), which ruptured the western portion of the NAF (Figure 1), was the largest earthquake in Turkey over the last 60 years. It was also the latest in a sequence of seven large earthquakes with mostly westward rupture migration along the NAF, starting with the 1939 Erzincan earthquake [e.g., Stein *et al.*, 1997]. Less than 3 months later, the Izmit earthquake was followed by the 12 November M_w 7.2 Düzce earthquake that ruptured a neighboring fault segment to the east of the Izmit rupture. It was suggested by Stein *et al.* [1997] and others that this sequence of earthquakes can be explained by a transfer of stresses from the ruptured fault segments to the adjacent segments. Calculations of stress triggering indicate that the segment below the Marmara Sea just west of the Izmit fault was brought closer to failure after the 1999 Izmit earthquake [e.g., Barka, 1999], which leads to

increases in the probability of strong shaking in the Istanbul metropolitan area [Parsons *et al.*, 2000].

[4] The 17 August 1999 Izmit earthquake has been subject to several geodetic studies. Reilinger *et al.* [2000] and Burgmann *et al.* [2002] used Global Positioning System (GPS) observations to determine the coseismic and post-seismic slip distribution along the fault. They argued that rapid afterslip mostly below the seismogenic zone best explains the observations of postseismic deformation and suggested that this rapid afterslip might have helped trigger the nearby 12 November M_w 7.2 Düzce earthquake. Hearn and Burgmann [2005] used the coseismic GPS data of Izmit earthquake to study the role of depth-dependent elasticity on the slip model. Studies of the coseismic fault slip due to the Izmit earthquake employed joint inversions of GPS and InSAR data [Feigl *et al.*, 2002; Cakir *et al.*, 2003], as well as teleseismic and strong motion data [Delouis *et al.*, 2002]. Cakir *et al.* [2003] used InSAR and GPS data along with field observations to estimate the coseismic and early postseismic slip on and below the seismic rupture. The inference of rapid afterslip mostly near the base of the seismogenic zone is in agreement with the work of Reilinger *et al.* [2000] and Burgmann *et al.* [2002]. Wright *et al.* [2001] used InSAR

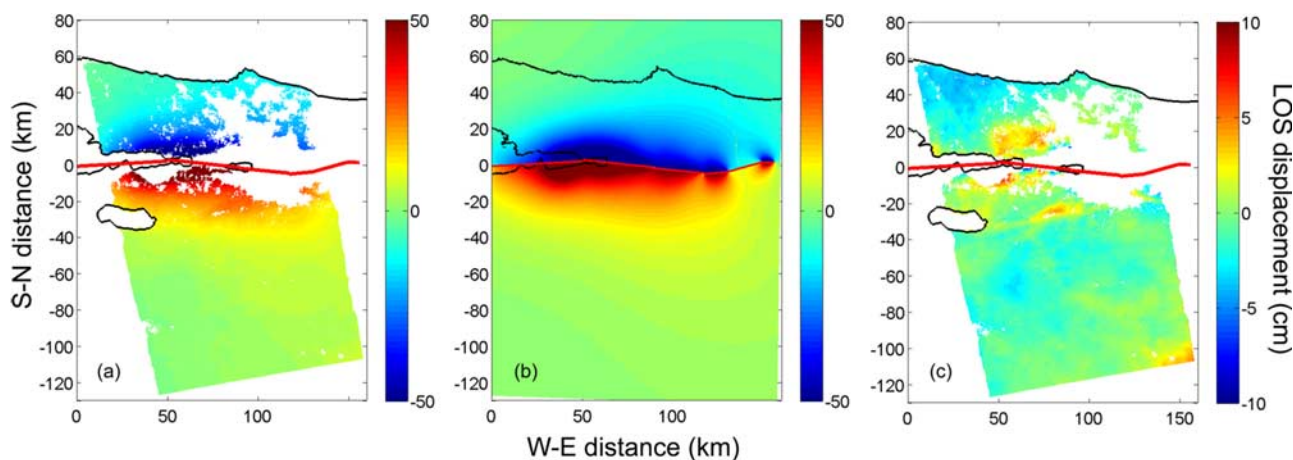


Figure 2. (a) Interferometric Synthetic Aperture Radar (InSAR) data for the Izmit earthquake collected by the ERS-1 satellite. The interferogram reveals the surface displacements, measured in the satellite's line-of-sight (LOS), for the time period 8 August to 16 September, 1999. (b) Synthetic interferogram derived from the InSAR data using the elastic layered model. The red line shows the location of the faults trace used to simulate the Izmit rupture. Details on the slip model, parameters are given in Tables 1 and 2. (c) Residual interferogram, obtained by subtracting the data (Figure 2a) from the model (Figure 2b). In all figures the origin corresponds to the Western limit of the Izmit rupture (29.19°E , 40.70°N), and the thick red line indicates the location of the modeled fault trace.

data to map the satellite line-of-sight displacement field of the Izmit earthquake and reported small-scale deformation anomalies away from the Izmit rupture, along nearby sub-parallel faults (in particular, the Mudurnu Valley and Iznik faults). *Wright et al.* [2001] interpreted the lineated anomalies in the radar range in terms of a shallow triggered slip on these faults. In order to match the observed changes in the radar range, *Wright et al.* [2001] suggested that a shallow triggered slip that does not reach the surface and has a sense that is opposite to the long-term geologic fault motion (i.e., left-lateral slip on right-lateral faults). Such retrograde slip may occur on nearby faults if the strength of these faults as well as the shear stress resolved on the fault plane is very low (of the order of the coseismic stress change). However, on the basis of mechanical grounds, such faults would be expected to slip all the way up to the surface. For example, such retrograde slip was reported on the Hayward fault that crept left-laterally for approximately 6 years following the Loma-Prieta earthquake, California [*Lienkaemper et al.*, 1997]. In this paper, we demonstrate that the inferred deformation anomalies along faults parallel to the Izmit rupture are consistent with an elastic response of compliant fault zones to the coseismic stress changes induced by the Izmit earthquake. The latter interpretation does not require any shallow retrograde slip on faults adjacent to the NAF.

2. Data Analysis and Inversion for Coseismic Slip Model

[5] To investigate stress changes induced by the Izmit earthquake in the surrounding crust, we begin by deriving the static rupture model. We use both SAR and GPS data in order to infer the slip distribution due to the Izmit earthquake. The SAR data provide a detailed scalar map of surface deformation in a 100-km wide swath covering the earthquake rupture, while the GPS data provide three-

component displacement data (albeit with reduced vertical precision) at selected locations both in the near and far field of the earthquake rupture. We use data from the ERS-1 and ERS-2 satellites of the European Space Agency to generate radar interferograms for the Izmit earthquake. The InSAR data that best capture the coseismic signal correspond to radar acquisitions made on 12 August to 16 September (ERS-1; perpendicular baseline, 57 m), and 13 August to 17 September (ERS-2; perpendicular baseline, 41 m). All SAR acquisitions used in this study are from the ERS ascending track 157, frames 815-797. Figure 1 outlines the respective ERS radar scene. The radar interferograms for the Izmit earthquake contain only 1 month of postseismic deformation, with pre-earthquake acquisition made 4 and 5 days before the earthquake. Thus, the postseismic deformation is expected to be relatively small compared to the coseismic deformation. The InSAR data were processed using ROI_PAC software. The coherence of the interferograms was found to be fairly good over most of the study area; however, the coherence is lost within large areas near to the fault trace, probably because of high degree of surface disruption and damage in the epicentral area. Figure 2a shows the coseismic line-of-sight (LOS) displacements obtained from the ERS-1 interferogram. White areas represent regions of decorrelation in the LOS displacement map. In addition to the LOS displacements, we estimate the range offsets by cross-correlating the radar amplitude between the two acquisitions along the range direction. The range offset data are less sensitive to changes in the reflective properties of the ground compared with the radar phase (LOS) data and therefore provide useful information on displacements near the fault trace. In particular, the range offset data helped us determine the location of the surface trace of the Izmit rupture. The location of the rupture trace inferred from the range offset data was found to be in a good agreement with the rupture location determined from the field studies.

Table 1. Izmit Subfault Model Used for the Inversion

Parameters	Segment 1	Segment 2	Segment 3	Segment 4	Segment 5	Segment 6
x_0 , km	25	70	103.5	123.5	139.5	152.5
y_0 , km	0.55	0.6	-3.35	-4.6	-1.35	1.25
Length, km	50	40	27.3	13	19.7	7
Dip, degrees	90	94	90	90	90	90
Strike, degrees	86.7	96	95.6	84.7	74.4	90.8

[6] The GPS data used in this study are taken from *Reilinger et al.* [2000] and *Burgmann et al.* [2002]. These authors estimated the coseismic displacement vectors using data collected from permanent, continuous GPS stations, as well as from survey-mode GPS measurements [*Straub et al.*, 1997; *McClusky et al.*, 2000]. Five of the continuous GPS stations were operating prior to the Izmit earthquake in the near field of the rupture. The total number of 51 GPS stations was resurveyed within the 2 weeks following the earthquake.

[7] The observed coseismic deformation can be generally explained by a simple model based on solutions for dislocations in an elastic half-space [e.g., *Savage and Hastie*, 1969; *Simons et al.*, 2002; *Fialko*, 2004]. Solutions for surface displacements due to dislocations in elastic half space are readily available for both homogeneous [e.g., *Okada*, 1985] and layered media [e.g., *Wang et al.*, 2003]. To assess the slip distribution on the Izmit rupture, we invert both the ERS InSAR and GPS data. The inversion scheme is based on a least squares minimization of the displacement misfit with iterations for the fault geometry [*Fialko*, 2004]. The initial fault geometry in our models was chosen using field observations of the surface rupture [*Cakir et al.*, 2003], as well as InSAR data; in particular, we use the range offset data, which provide detailed information on the location of the fault trace and the fault offset. To account for the nonplanar geometry of the surface rupture, we divide the fault trace into six rectangular segments. The initial segments were chosen to be vertical rectangles having downdip dimension of 20 km. Subsequently, we refined the fault plane geometry by allowing small changes in the fault dip (up to 6° from vertical) in order to minimize the data misfit in a nonlinear least squares inversion. Details on the best fitting segment geometry are given in Table 1. To evaluate the spatial distribution of the fault slip, each segment was further subdivided into patches of $4 \times 5 \text{ km}^2$ each, with constant slip on each patch. We calculated the slip distribution assuming homogeneous and layered half-space models. For the homogeneous half-space model, each patch was approximated by a finite rectangular dislocation [*Okada*, 1985], while for the layered half-space model, each patch was approximated by a dense array of point dislocations with equal slip [*Wang et al.*, 2003]. We found only small variations between the homogeneous half-space and the layered-media inversions results, in both the slip model and the surface deformation. Therefore, in this paper, we present results of only one inversion corresponding to the layered half-space. The elastic moduli structure used in our layered half-space model is given in Table 2. This structure is based on the seismic velocity model for the area presented by *Gurbüz et al.* [2003]. The extensive radar decorrelation around the Izmit rupture results in the loss of continuity of the radar phase between the northern and southern parts of the interfero-

grams. We find a constant offset between areas separated by decorrelation as part of our inversion. The constant offset represents an integer number of phase cycles between select fringes on both sides of the decorrelation zone. This approach a priori minimizes any potential asymmetry in the coseismic surface displacements (e.g., due to material contrasts, see the work of *Fialko* [2006]) across the NAF.

[8] Figure 3 shows the slip distribution inferred from our layered half-space inversion. The inferred slip is predominantly right lateral, however, the slip model also reveals some small-scale dip-slip motion, up to 50 cm, mainly in the westernmost segment of the earthquake rupture. Our slip model indicates that most of the coseismic slip during the Izmit earthquake occurred in the central part of the fault plane, up to about 40 km both eastward and westward from the epicenter. According to our slip model, the total seismic moment release is $M_0 = 2.3 \times 10^{20} \text{ N}\cdot\text{m}$ (corresponding to a moment magnitude $M_w = 7.5$), which is somewhat higher than the estimated moment derived from broadband teleseismic data ($M_0 = 1.3\text{--}1.7 \times 10^{20} \text{ N}\cdot\text{m}$; e.g., *Li et al.* [2002]), but consistent with moment estimates from other geodetic studies [*Reilinger et al.*, 2000; *Delouis et al.*, 2002; *Cakir et al.*, 2003; *Hearn and Burgmann*, 2005], as well with moment estimates based on the near-field seismological data [*Bouchon et al.*, 2002]. It should be noted that the InSAR data include 1 month of postseismic deformation, including aftershocks (with M_d 5.8 event being the largest aftershock), which probably gives rise to a higher estimated moment release. The overall calculated slip near the surface is consistent with field observations along a large surface rupture between Sapanca and slightly west to Golcuk [*Barka et al.*, 2002; *Rockwell et al.*, 2002, *Aydin and Kalafat*, 2002]. The slip model is also found to be in a general agreement with other geodetic models [*Reilinger et al.*, 2000; *Burgmann et al.*, 2002; *Cakir et al.*, 2003], indicating that most of the slip occurred in the central part of rupture, between Hersek and Sapanca segments, with some additional slip up to 3 m (2.2 m in our model) on the eastern Karadere segment. The calculated surface displacements in the observed and residual (i.e., data minus model) line-of-sight displacements are presented in Figures 2b and 2c, respectively. A comparison between the GPS data and the calculated displacement vectors in the locations of the GPS stations is shown in Figure 4. As one can see in Figures 2c and 4, there is a good agreement between

Table 2. Variation in the Elastic Moduli With Depth Used for the Elastic Layered Model

Depth, km	Shear Modulus, GPa	Poisson Ratio
0–1	15.6	0.30
1–5	29.4	0.18
5–32	38.3	0.25
>32	61.0	0.26

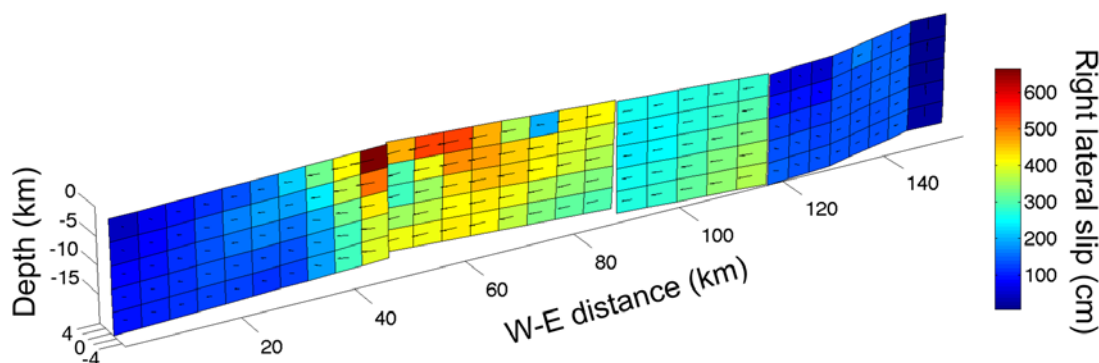


Figure 3. The modeled right-lateral slip distribution from the inversion of SAR and GPS data for the elastic layered model. The small black arrows indicate the direction and amplitude of slip for every patch.

both InSAR and GPS data and the surface displacements calculated from our slip model.

3. Coseismic Deformation Along Nearby Faults

[9] The residual displacements map (Figure 2c) reveals small-scale yet systematic anomalies along geologically mapped faults away from the Izmit rupture. These anomalies can be due to tropospheric effects or geological heterogeneity (such as variable rock properties), giving rise to local variations in the radar phase, or a local misfit between the observed deformation and that calculated using homogeneous elastic models. In order to check if the surface anomalies are due to tropospheric effects, we processed the 1-day tandem interferograms that do not include the coseismic signal for both August and September acquisitions. To isolate the localized anomalies, we detrended the 1-day interferograms by subtracting the best fitting bilinear surface. The detrended tandem interferograms for August and September are presented in Figures 5a and 5b, respectively. As one can see in Figure 5, there is no clear correlation between the 1-day interferograms and the residual coseismic changes in the radar range (Figure 2c), especially where the localized anomalies are observed. For example, the LOS displacements in the 1-day interferograms along profile A-A', B-B', and C-C' have only small and gradual variations between ± 1 cm. Below, we will further discuss the residual coseismic changes along these profiles. The absence of lineated anomalies in 1-day interferograms, as well as a remarkable consistency of such anomalies in the two independent 1-month interferograms, suggests that atmospheric artifacts (in particular, water vapor) are not a likely cause of the observed variations in the residual LOS displacements and that these displacements may be due to the coseismic deformation.

[10] Figure 6 illustrates the location of the localized anomalies south of the main rupture; also shown is the location of mapped faults in this area [Saroglu *et al.*, 1992; Aydin and Kalafat, 2002; Barka *et al.*, 2002]. Figure 7 shows the observed LOS displacements for both coseismic interferograms (12 August to 16 September for ERS-1, and 13 August to 17 September for ERS-2 interferograms) and the topography along profile A-A'. The LOS displacement anomaly along profile A-A' is of the order of 4 cm. The imperfect correlation between the LOS displacements and the topography profiles lends further support to our sug-

gestion that the observed anomaly is related to the coseismic deformation and not to atmospheric effects (as one might expect, for example, in case of a stratified moisture distribution). As shown in Figure 6, the deformation anomalies occur along nearby faults of the North Anatolian Fault system (the Mudurnu Valley and Izmit faults). Wright *et al.* [2001] interpreted these deformation anomalies as being due to retrograde triggered shallow slip on the Mudurnu Valley and Izmit faults. However, the aftershock data indicate a right-lateral slip (usually with some normal component) along these and other subparallel faults in the area [Dziawonski *et al.*, 2000], and there is no independent evidence for left-lateral motion along the Mudurnu Valley (profile A-A') and Izmit (profile B-B') faults. Furthermore, it may be argued that a shallow retrograde slip that does not reach the surface is unlikely, and alternative explanations are possible [Fialko *et al.*, 2002; Fialko, 2004]. Here we demonstrate that the small-scale LOS anomalies along the Mudurnu and Izmit faults (Figure 6) can be explained by assuming that the faults are surrounded by wide damage zones that have different mechanical properties compared to

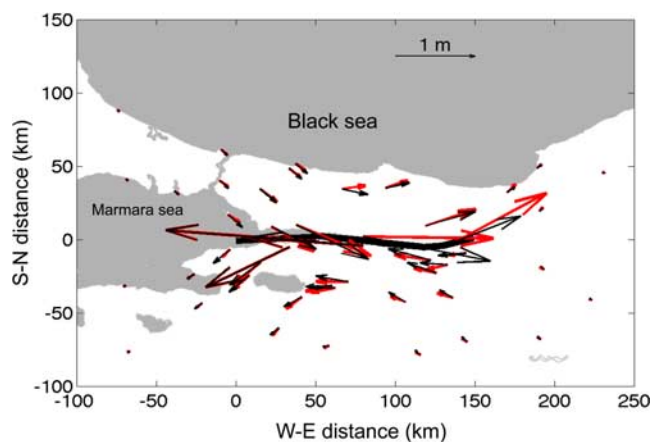


Figure 4. A comparison between the horizontal coseismic displacements observed with GPS (red arrows) and predicted by our slip model (black arrows). Thick black line indicates the location of the modeled fault trace. The observed coseismic displacements are relative to a station (ANKR, located at 39.89°N, 32.76°E) in Ankara, Turkey [Reilinger *et al.*, 2000].

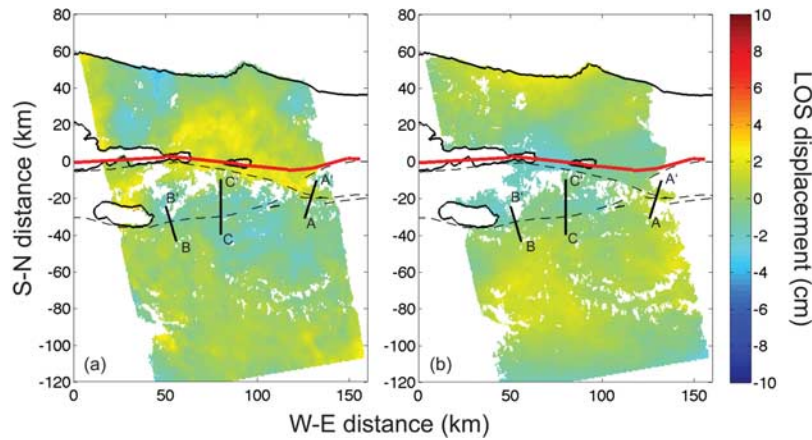


Figure 5. Tandem interferograms from ERS-1 and ERS-2 satellite acquisitions. (a) 12–13 August 1999 (perpendicular baseline, 236 m) (b) 16–17 September 1999 (perpendicular baseline, 252 m). Dashed lines indicate the location of the mapped segments of the North Anatolian Fault zone. To isolate localized anomalies, a ramp at the scale of one entire interferogram was removed from the data. The red line shows the location of the faults trace used to simulate the Izmit rupture.

the host rocks and therefore have a distinct elastic response to the static stress change because of a nearby earthquake.

[11] In order to evaluate the elastic response of a compliant fault zone to the coseismic stress field, we performed three-dimensional numerical simulations using the finite element code ABAQUS. To mimic the behavior of a compliant fault zone around a strike-slip fault, a vertical low rigidity layer was introduced in the middle of an elastic block. The latter is assumed to have shear modulus of $G = 30$ GPa in our simulations. On the boundaries of this block we applied the inferred change in the static stress field deduced from our slip model for the Izmit earthquake. Next, we calculated the surface deformation for a variety of fault zone properties. The shear and normal stresses resolved on a fault striking in the E-W direction (as inferred from our slip model) are presented in Figure 8. The calculations shown in Figure 8 correspond to a depth of 2 km, with extensional and right-lateral shear stress changes considered to be positive. A comparison between the calculated and observed LOS displacements is performed along profiles A-A' (Mudurnu Valley fault) and B-B' (Iznik fault) in Figure 6. According to our slip model for the Izmit earthquake, the normal stress change on the Mudurnu Valley fault is 0.6 MPa and the shear

stress change is 0.3 MPa (see profile A-A'). For the Iznik fault, the inferred normal stress change is 0.2 MPa and the shear stress change is 0.15 MPa (profile B-B'). Figure 9 shows the comparison between the calculated and observed LOS displacements along profile A-A' for calculations with different fault zone width (Figure 9a), fault zone depth (Figure 9b), and rigidity reduction (Figure 9c). As one can see in Figure 9, the magnitude of the theoretically predicted anomaly increases with increasing the fault zone width, depth, and rigidity reduction; however, the model predictions are relatively insensitive to increases in the fault zone depth in excess of more than ~ 10 km (Figure 9b). Thus, one cannot distinguish between the elastic response of a fault zone that extends to depths of, for example, 10 and 20 km. Figure 9d shows the predicted vertical and horizontal deformation in the LOS direction for the case of 3-km fault zone width, 10-km fault zone depth, and a rigidity ratio of 1/3. The response of a compliant zone measured with InSAR depends on both the normal and shear stress changes and therefore will be affected by the ratio between these stress changes. Figure 9d indicates that in case of profile A-A', the normal and shear stress changes have comparable contribution to the total deformation. According to a comparison presented in

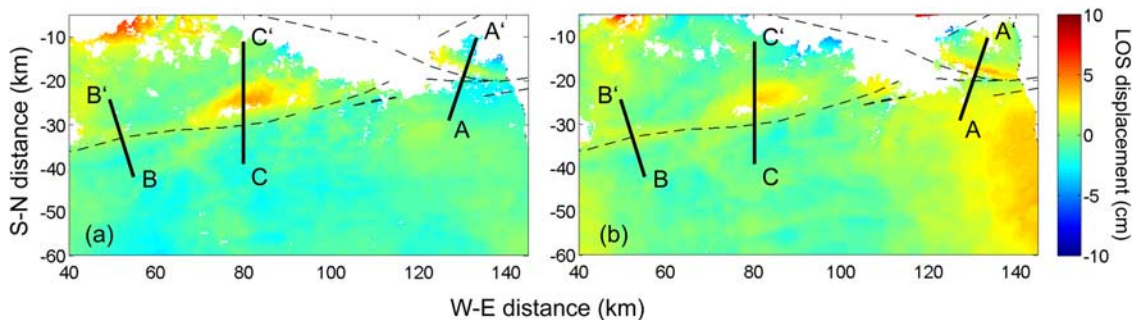


Figure 6. Residual interferograms from (a) ERS-1 and (b) ERS-2 coseismic interferograms for the area of Mudurnu Valley and Iznik faults south to the Izmit rupture. Dashed lines denote mapped segments of the North Anatolian Fault zone. The anomalies in the LOS displacements are spatially correlated with the preexisting faults.

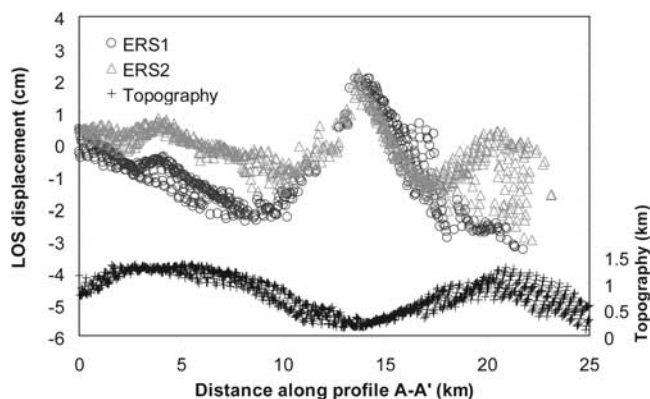


Figure 7. The residual LOS displacements from the ERS-1 (black circles) and ERS-2 (gray triangles) interferograms (upper curves), and topography (lower curve) along profile A-A'.

Figure 9, the model that best fits both interferometric (i.e., ERS-1 and ERS-2) data sets is a model with a fault zone having a characteristic width of 2–3 km, depth extent of 10 km (or more), and shear modulus reduction of about a factor of 3 relative to the shear modulus of the ambient crust. Figure 10 presents a comparison between the calculated and observed LOS displacements for both interferograms (ERS-1 and ERS-2) along profile B-B'. The calculated displacements presented in Figure 10 are for fault zone width of 2 and 3 km, depth of 20 km, and a shear modulus reduction of a factor of 3. Note that the results for the Iznik fault are quite consistent with those for the Mudurnu Valley fault (profile A-A').

[12] Relatively large residual deformation is observed along the middle segment of the Iznik fault (profile C-C'; Figure 6). Figure 11 illustrates the LOS displacement data from the ERS-1 and ERS-2 interferograms along profile C-C'. As shown in the figure, the magnitude of the deformation anomaly along profile C-C' is of the order of 5 cm, and the width of the anomaly (~ 15 km) is much larger than the width of the fault zones deduced for profiles A-A' and B-B'. In order to understand the nature of a large residual along profile C-C', we developed a fully three-dimensional model using the Fast Lagrangian Analysis of Continua algorithm [Cundall, 1989; Hamiel *et al.*, 2004]. The numerical simulation includes an elastic block that represents an area of 160×70 km² south to the main rupture, divided into tetrahedral elements generated with the TetGen code (by Hang Si from Weierstrass Institute for Applied Analysis and Stochastics). A low rigidity zone that extends to the depth of the block (20 km) and is approximately 3 km wide, depending on the local mesh geometry, was introduced along the location of all the mapped faults in the area (Figure 1). The shear modulus of the compliant zone was assumed to be a factor of 3 smaller than that of the surrounding rock, consistent with the best fitting results for profiles A-A' and B-B'. At the beginning of the simulation, the stress was prescribed within the block on the basis of predictions from our slip model for the Izmit earthquake. Subsequently, we calculated the elastic response of the entire block with and without the compliant zones. Figure 11a shows a map view of the difference in LOS displacements between the simulations with and without the compliant zones, and Figure 11b shows

a comparison between the observed and predicted data by our model along profile C-C'. As one can see in Figures 11a and 11b, our model shares a number of qualitative similarities with the data and is consistent with the overall observed deformation in the area; however, the observed LOS displacement anomaly differs in some places from the calculated one. Several reasons may be responsible for this difference between the calculated and observed deformation. First reason for this difference may be the existence of local secondary or inactive faults surrounded by low rigidity zones, as well as local sedimentary basins with low rigidity fill that were not taken into account in our model. It should be noted that the latter accounts for only the major active faults in the area. Second reason can be due to variations in the fault zone width, depth, and rigidity contrast along the modeled faults. Third reason for the difference between the observed and modeled LOS displacements along profile C-C' might be the atmospheric noise. Figure 11b shows the topography along profile C-C'. Although the anomalous range changes do not perfectly follow the local topography, there is a certain

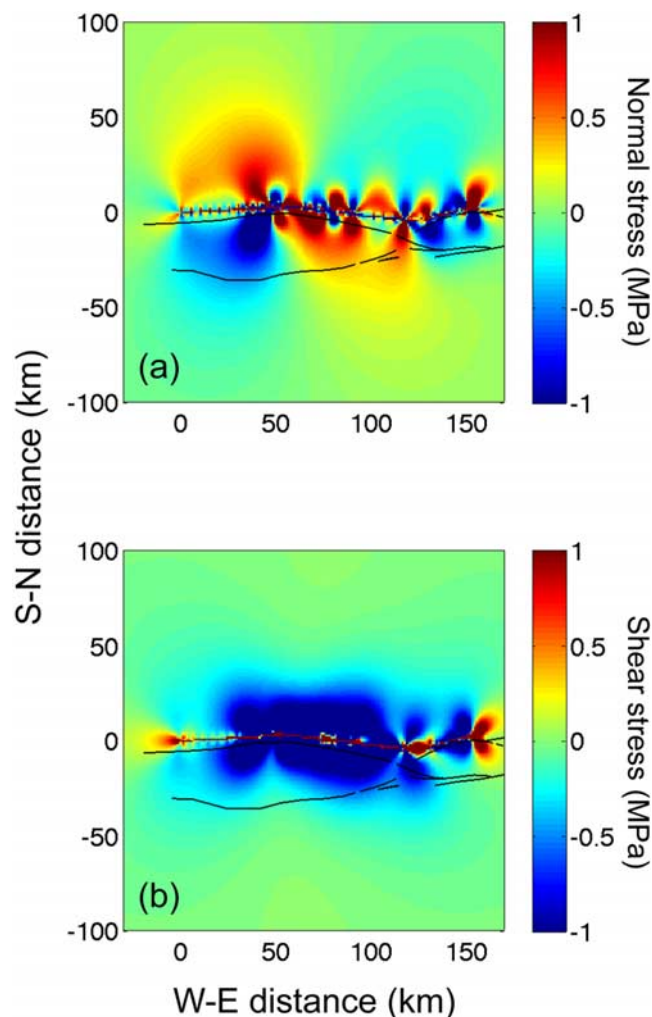


Figure 8. (a) Static normal and (b) shear stress changes due to the Izmit earthquake, in megapascals, at the depth of 2 km on vertical fault striking in E-W direction (the general direction of the Izmit rupture). Extensional and right-lateral shear stress changes are considered to be positive.

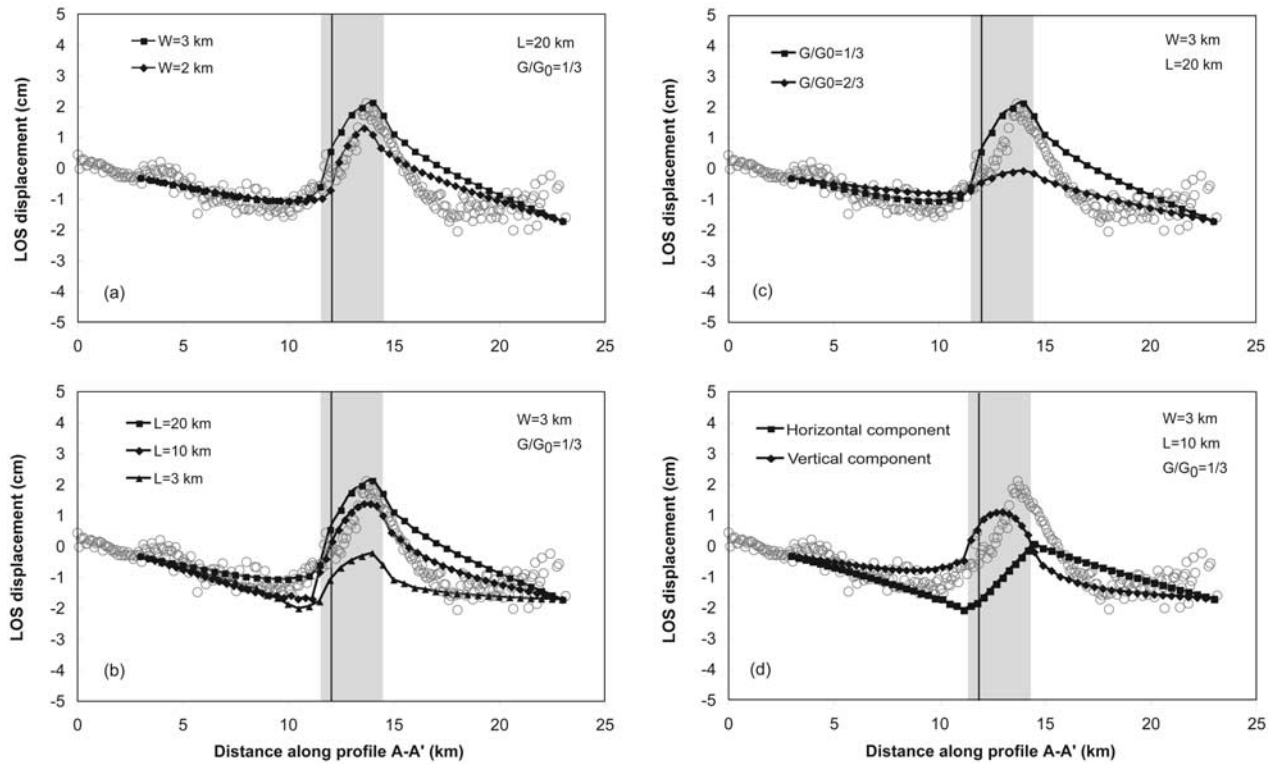


Figure 9. A comparison between the average residual LOS displacements (gray circles) from ERS-1 and ERS-2 interferograms and the calculated displacements from the three-dimensional finite element model along profile A-A'. Calculated curves for different (a) width (W), (b) length (L), and (c) shear modulus (G) of the fault zone. The gray areas indicate the locations of the 3-km-wide modeled fault zone, and the black lines indicate the locations of the geologically mapped fault trace. The best fitting curves correspond to fault zones that are 2–3 km wide; extend to the depth of 10–20 km, and have shear moduli ratio of $\sim 1/3$. (d) The predicted horizontal and vertical deformation projected to the LOS direction for the case of $W = 3$ km, $L = 10$ km, and $G / G_0 = 1/3$. This figure indicates that the normal and shear stress changes contribute equally to the total displacements along profile A-A'.

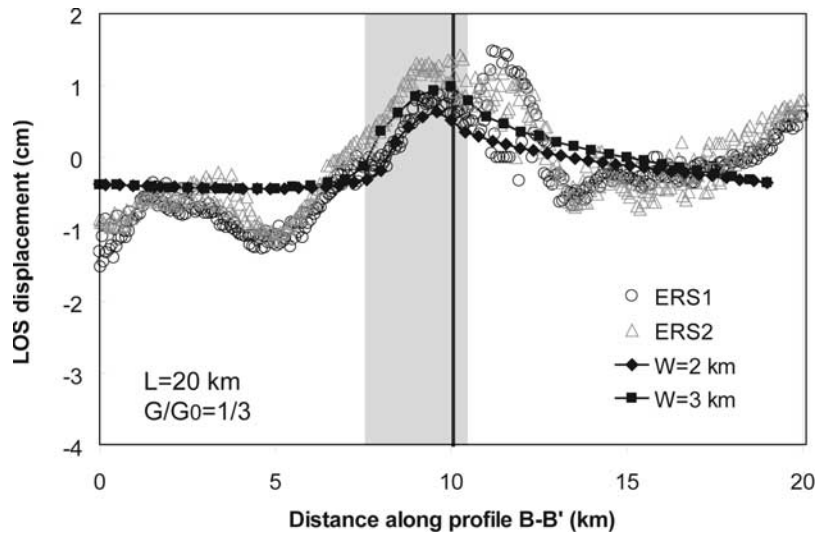


Figure 10. A comparison between the residual LOS displacements from ERS-1 (black circles) and ERS-2 (gray triangles) interferograms and the calculated displacements from the three-dimensional finite element model along profile B-B'. The gray area indicates the location of the 3-km-wide modeled fault zone, and the black line indicates the location of the geologically mapped fault trace. The calculations are for a fault zone that extends to the depth of 20 km and has shear moduli ratio of $1/3$. The different theoretical curves represent different fault zone width (2 and 3 km).

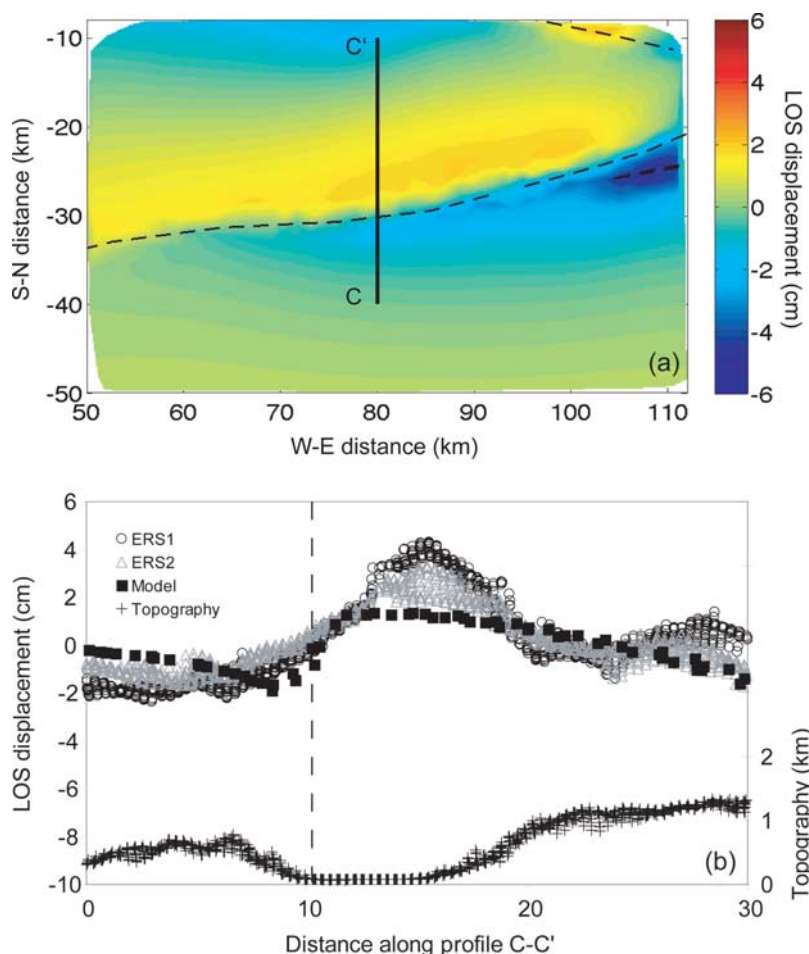


Figure 11. (a) A map view of the modeled LOS displacement from a three-dimensional numerical model in the region of profile C-C'. Dashed black line indicates the location of the mapped faults and the modeled compliant zones in the area. This model includes the stress distribution due to the Izmit earthquake and fault zones at the location of the faults that are approximately 3 km wide, extend to the depth of 20 km, and have shear moduli ratio of 1/3. (b) A comparison between the residual LOS displacements from ERS-1 (black circles) and ERS-2 (gray triangles) interferograms and the calculated displacements shown in Figure 11a along profile C-C'. Dashed black line indicates the location of the mapped fault along the profile.

correlation between the location of the anomaly and the location of the basin, and the amplitude of the anomaly somewhat varies between the two interferograms. Some deformation may be attributed to aftershock activity, as this area has produced significant seismicity over the time period of 1 month following the Izmit earthquake, with two largest aftershocks having magnitudes between 4 and 5 and two additional aftershocks with magnitudes between 3 and 4 (data from the local Turkish network, General Director of Disaster Affairs Earthquake Research Department website: www.deprem.tr) that occurred between the two SAR acquisitions. These aftershocks could have altered the local stress field and caused an additional surface deformation. Finally, we point out that a negative anomaly to the east of profile C-C' (UTM easting of 100–110 km, Figure 11a) predicted by our model is due to a very large compliant structure at the junction of two merging faults (see dashed black lines in Figure 11a). Our model assumes that each fault is associated with a 3-km-wide damage zone, which

gives rise to a total width of the compliant zone of 6 km near the fault junction. The extent of damage in such a structurally complex may be overestimated in our model.

4. Discussion

[13] We analyzed the coseismic deformation induced by the 17 August 1999 Izmit earthquake using space geodetic observations. The InSAR data include two coseismic interferograms, with preseismic acquisitions made several days before the Izmit earthquake, and repeat acquisitions made about a month after the earthquake. On the basis of the GPS and InSAR data, we developed a slip model for the Izmit earthquake. The surface displacement field predicted by our model is in an overall agreement with the observed one. However, the InSAR data reveal some small LOS displacement anomalies away from the Izmit rupture, along nearby faults of the NAF system (Mudurnu Valley and Iznik faults). These LOS displacement anomalies are consistent with an

elastic response of compliant fault zones to the coseismic stress change induced by the Izmit earthquake. On the basis of three-dimensional numerical simulations using finite element method, we found that the inferred fault zones have a characteristic width of 2–3 km, extend to depth of 10–20 km, and their rigidity is reduced by approximately 66% (the equivalent S wave velocity reduction of approximately 45%).

[14] Our results appear to be consistent with the structure and mechanical properties of fault zones in the Eastern California Shear Zone reported by *Fialko et al.* [2002] and *Fialko* [2004]. On the basis of InSAR observations of coseismic deformation due to the 1992 Landers and 1999 Hector Mine earthquakes, these authors argued that several faults adjacent to the earthquake ruptures have macroscopic damage zones with rigidity reduction of $\sim 50\%$, and width of approximately 2 km. *Cochran et al.* [2006] conducted a seismic experiment to investigate the structure and mechanical properties of a fault zone around the Calico fault of the Eastern California Shear Zone at the same location where InSAR observations were interpreted and indicating a large compliant fault zone. Preliminary results from the Calico fault seismic experiment reveal a 1- to 2-km-wide low velocity zone and a velocity reduction consistent with that inferred from the space geodetic measurements [*Fialko et al.*, 2002; *Fialko*, 2004].

[15] The characteristic width of fault zones determined in this study is also in agreement with field observations in the North Anatolian Fault area by *Ambraseys* [1970]. The latter study argues that the fault zones of the North Anatolian Fault system are broad belts of crushed rocks a few kilometers wide rather than localized narrow slip surfaces in an otherwise intact crust. *Ambraseys* [1970] also concluded that surface ruptures during an earthquake do not always follow precisely earlier breaks and mapped faults but seem to follow a path of “least resistance” within a broad zone of cracked rocks, a few hundreds of meters to a few kilometers wide. Our inferences of the effective rigidity reduction of 60–70%, corresponding to the S wave velocity reduction of $\sim 45\%$, are consistent with the velocity reduction along the North Anatolian Fault reported by *Ben-Zion et al.* [2003]. On the basis of seismic data of trapped waves recorded within the 6 months following the Izmit earthquake, *Ben-Zion et al.* [2003] studied the structure of the Karadera-Dunze segment of the NAF (the easternmost segment that ruptured during the Izmit earthquake). Their study suggests that the S wave velocity reduction is $\sim 50\%$, albeit within a narrower (~ 100 m) and shallower (3- to 4-km depth) fault zone compared to the fault zone geometries inferred for the Mudurnu Valley and Iznik faults in this study. We point out that the fault zone geometry and mechanical properties may vary substantially both across and along fault strike, as well as with depth. Variations in the effective width of a fault zone from tens to hundreds of meters to kilometers may not be unusual for major crustal faults [*Ambraseys*, 1970; *Li et al.*, 1994; *Chester and Chester*, 1998; *Fialko et al.*, 2002; *Fialko*, 2004; *Ben-Zion and Sammis*, 2003; *Cochran et al.*, 2006].

[16] The size of the observed anomaly along fault zones depends on the coseismic stress change, the fault zone width, depth, and the rigidity reduction with respect to the surrounding rocks. The coseismic stress change is a function of distance from the main rupture. The fault zone

width, depth, and the rigidity reduction are affected by the damage accumulated from previous slip events on the fault [*Ambraseys*, 1970]. Since the fault zone may heal between earthquakes, the rigidity reduction may be also affected by a time lapse since the last earthquake. Therefore one may expect that only large damage zones with a significant reduction in rigidity with respect to the surrounding rocks may produce geodetically detectable strain localization, provided that such damage zones experience sufficiently large stress changes (for example, are located in the near field of major earthquakes).

[17] The deduced rigidity reduction around large faults along ECSZ and the NAF can be associated with the existence of highly fractured zones. Linear and nonlinear expressions for the relations between the rigidity reduction and crack density have been suggested (e.g., see a review by *Kachanov* [1992]), but their experimental verifications have been rather limited. Recently, *Hamiel et al.* [2006] studied the relations between the rock rigidity and crack density using a visco-elastic damage rheology model and a direct microscopic mapping of cracks. The damage rheology approach is based on the assumption that the density of cracks is uniform over a length scale that is much larger than the length of a typical crack yet much smaller than the size of the entire deforming domain. For a system with a sufficiently large number of cracks, one can define a representative volume in which the crack density is uniform and introduce an intensive damage variable for this volume. According to damage mechanics, changes in the intensity of the damage variable are proportional to changes in the rock rigidity. *Hamiel et al.* [2006] tested the visco-elastic damage rheology against sets of laboratory experiments done on Mount Scott granite. On the basis of fitting of the entire stress-strain records, the damage variable was constrained and found to be a linear function of the crack density [*Hamiel et al.*, 2006, equation (8)]. This linear relation between the damage variable and crack density was found to be in agreement with the theoretical prediction of *Kachanov* [1992] and with a previous comparison between the calculated rate of damage accumulation and measured acoustic emission [*Hamiel et al.*, 2004]. Since the damage variable and the crack density characterize a properly chosen volume of rock with a large number of internal flaws (micro-cracks in a laboratory specimen or small faults in the Earth's crust) and are not related to any intrinsic length scale, *Hamiel et al.* [2006] suggested that the linear relation between the damage variable and crack density should be scale independent and hold on a scale of the thickness of the brittle crust. On the basis of this assumption, one can estimate changes in the effective shear modulus, G , as a function of the crack density, ρ_c . The crack density is defined as the sum of squared length of all the mapped cracks normalized by the representative area, A :

$$\rho_c = \frac{1}{A} \sum_n l_n^2 \quad (1)$$

where l_n is the half-length of the cracks. Figure 12 shows the relation between the shear modulus and the measured crack density based on laboratory tests on Mount Scott granite [*Hamiel et al.*, 2006]. As shown in Figure 12, linear

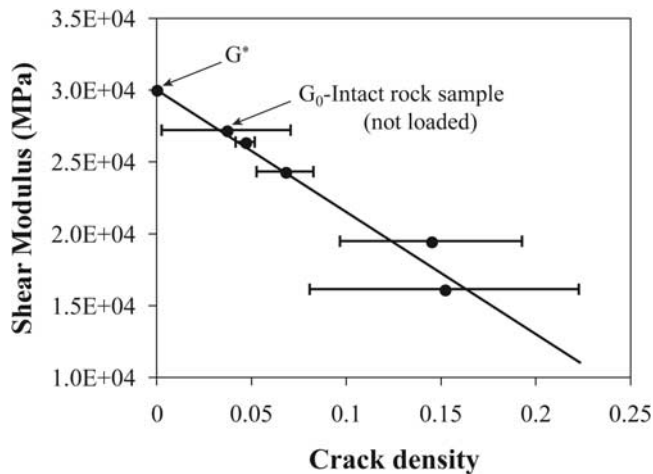


Figure 12. The measured crack density, ρ_c , versus the calculated shear modulus, G , in experiments with Mount Scott granite. The inferred linear relation, $G = G^* - 8.5 \times 10^4 \rho_c$ (in MPa), is shown by a black line.

regression provides a reasonable relation between the crack density and the shear modulus:

$$G = G^* - 8.5 \times 10^4 (\pm 1.5 \times 10^4 \text{ Mpa}) \rho_c \quad (2)$$

On the basis of nine different sets of experiments, $G^* = G(\rho_c = 0) = 3 \times 10^4$ MPa is inferred to be the shear modulus of the undamaged Mount Scott granite. Note that the crack density of the intact rock sample (that is, the sample that was not loaded) is not 0. The suggested linear relation between the shear modulus (or damage) and crack density does not imply a linear Hookean elasticity. The model of Hamiel et al. [2004, 2006] includes a nonanalytical, second-order term in the energy expression, in addition to the quadratic terms representing the Hookean elastic solid. Thus, this model accounts for the crack dilation and closure due to changes in the crack-normal stress and leads to nonlinear stress-strain relations even for small strains. Using a linear relation between the shear modulus and the crack density [see equation (2)], one can evaluate changes in the crack density between the fault zone and the surrounding rock. Variations in the effective shear modulus between the fault zone and the surrounding rock of a factor of 2 to 3 (suggested by this study for faults in the North Anatolian Fault system and by previous studies for faults in the Eastern California Shear Zone), the average crack density in the fault zone is estimated to be approximately five to seven times larger than the crack density in the surrounding rock. Our inference of a finite fault zone with high crack density is in agreement with recent field observations of highly fractured rock along large crustal faults [e.g. Ben-Zion and Sammis, 2003; Peng and Ben-Zion, 2004; Wilson et al., 2005; Chester et al., 2005].

[18] **Acknowledgments.** We thank V. Lyakhovskiy for useful discussions. We also would like to thank P. Taylor, T. Dixon, R. Burgmann, and an anonymous reviewer for their constructive remarks on an early version of the manuscript. The authors gratefully acknowledge support from the Green Foundation (Y.H.), the National Science Foundation (grant EAR-

0450035 made to Y.F.), and the Southern California Earthquake Center (SCEC). The SCEC contribution number for this paper is 1072.

References

- Alm, O., L. L. Jaktlund, and S. Kou (1985), The influence of microcrack density on the elastic and fracture mechanical properties of Stripa granite, *Phys. Earth. Planet. Inter.*, *40*, 161–179.
- Ambraseys, N. N. (1970), Some characteristic features of the Anatolian Fault Zone, *Tectonophysics*, *9*, 143–165.
- Armijo, R., B. Meyer, A. Hubert, and A. Barka (1999), Westward propagation of the North Anatolian Fault into the northern Aegean: Timing and kinematics, *Geology*, *27*, 267–270.
- Aydin, A., and D. Kalafat (2002), Surface ruptures of the 17 August and 12 November 1999 Izmit and Duzce earthquakes in Northwestern Anatolia, Turkey: Their tectonic and kinematic significance and the associated damage, *Bull. Seismol. Soc. Am.*, *92*, 126–137.
- Barka, A. (1999), The 17 August 1999 Izmit earthquake, *Science*, *285*, 1858–1859.
- Barka, A., et al. (2002), The surface rupture and slip distribution of the 17 August 1999 Izmit earthquake (M 7.4), North Anatolian Fault, *Bull. Seismol. Soc. Am.*, *92*, 43–60.
- Ben-Zion, Y., and C. G. Sammis (2003), Characterization of fault zones, *Pure Appl. Geophys.*, *160*, 677–715.
- Ben-Zion, Y., Z. Peng, D. Okaya, L. Seeber, J. G. Armbruster, N. Ozer, A. J. Michael, S. Baris, and M. Aktar (2003), A shallow fault zone structure illuminated by trapped waves in the Karadere-Duzce branch of the North Anatolian Fault, western Turkey, *Geophys. J. Int.*, *152*, 699–717.
- Bouchon, M., M. N. Toksoz, H. Karabulut, M. P. Bouin, M. Dietrich, M. Aktar, and M. Edie (2002), Space and time evolution of rupture and faulting during the 1999 the Izmit (Turkey) earthquake, *Bull. Seismol. Soc. Am.*, *92*, 256–266.
- Budiansky, B., and R. J. O'Connell (1976), Elastic moduli of a cracked solid, *Int. J. Solids Struct.*, *12*, 81–97.
- Burgmann, R., S. Ergintav, P. Segall, E. H. Hearn, S. McClusky, R. E. Reilinger, H. Woith, and J. Zschau (2002), Time-dependent distributed afterslip on and deep below the Izmit rupture, *Bull. Seismol. Soc. Am.*, *92*, 126–137.
- Cakir, Z., J. B. de Chabaliere, R. Armijo, B. Meyer, A. Barka, and G. Peltzer (2003), Coseismic and early postseismic slip associated with the 1999 Izmit earthquake (Turkey), from SAR interferometry and tectonic field observations, *Geophys. J. Int.*, *155*, 93–110.
- Chester, F. M., and J. S. Chester (1998), Ultracataclastic structure and friction processes of the San Andreas Fault, *Tectonophysics*, *295*, 199–221.
- Chester, J. S., F. M. Chester, and A. K. Kronenberg (2005), Fracture surface energy of the Punchbowl fault, San Andreas system, *Nature*, *437*, 133–136.
- Cochran, E. S., M. Radiguet, P. M. Shearer, Y.-G. Li, Y. Fialko, and J. E. Vidale (2006), Seismic imaging of the damage zone around the Calico Fault, *Eos Trans. AGU*, Fall Meet. Suppl.
- Cundall, P. A. (1989), Numerical experiments on localization in frictional materials, *Ing.-Arch.*, *59*, 148–159.
- Delouis, B., D. Giardini, P. Lundgren, and J. Salichon (2002), Joint inversion of InSAR, teleseismic and strong motion data for the spatial and temporal distribution of earthquake slip: Application to 1999 Izmit main shock, *Bull. Seismol. Soc. Am.*, *92*, 278–299.
- Dziewonski, A. M., G. Ekstrom, and N. N. Maternovskaya (2000), Centroid-moment tensor solutions for July–September 1999, *Phys. Earth Planet. Inter.*, *119*, 311–319.
- Feigl, K. L., et al. (2002), Estimating slip distribution for the Izmit main-shock from coseismic GPS, RADARSAT, ERS-1, and SPOT measurements, *Bull. Seismol. Soc. Am.*, *92*, 138–160.
- Fialko, Y. (2004), Probing the mechanical properties of seismically active crust with space geodesy: Study of the co-seismic deformation due to the 1992 $M_w 7.3$ Landers (southern California) earthquake, *J. Geophys. Res.*, *109*, B03307, doi:10.1029/2003JB002756.
- Fialko, Y. (2006), Interseismic strain accumulation and the earthquake potential on the southern San Andreas fault system, *Nature*, *441*, 968–971.
- Fialko, Y., D. Sandwell, D. Agnew, M. Simons, P. Shearer, and B. Minster (2002), Deformation on nearby faults induced by the 1999 Hector Mine earthquake, *Science*, *297*, 1858–1862.
- Gurbüz, C., T. Bekler, M. N. Toksoz, S. Kuleli, Dogan Kalafat, and C. A. Schultz (2003), Seismic refraction studies and crustal structure in Anatolia, *Commission on Controlled-Source Seismology: Deep Seismic Methods, 12th International Workshop*, Virginia, USA.
- Hadley, K. (1976), Comparison of calculated and observed crack densities and seismic velocities in Westerly granite, *J. Geophys. Res.*, *81*, 3484–3494.

- Hamiel, Y., Y. Liu, V. Lyakhovskiy, Y. Ben-Zion, and D. Lockner (2004), A visco-elastic damage model with applications to stable and unstable fracturing, *J. Geophys. Int.*, *159*, 1155–1165.
- Hamiel, Y., O. Katz, V. Lyakhovskiy, Z. Reches, and Y. Fialko (2006), Stable and unstable damage evolution in rocks with implications to fracturing of granite, *Geophys. J. Int.*, *167*, 1005–1016.
- Hearn, E. H., and R. Burgmann (2005), The effect of elastic layering on inversions of GPS data for coseismic slip and resulting stress changes: Strike-slip earthquakes, *Bull. Seismol. Soc. Am.*, *95*, 1637–1653.
- Kachanov, M. (1992), Effective elastic properties of cracked solids: Critical review of some basic concepts, *Appl. Mech. Rev.*, *45*, 304–335.
- Katz, O., and Z. Reches (2004), Microfracturing, damage, and failure of brittle granites, *J. Geophys. Res.*, *109*, B01206, doi:10.1029/2002JB001961.
- Li, Y. G., K. Aki, D. Adams, A. Hasemi, and W. H. K. Lee (1994), Seismic guided waves trapped in the fault zone of the Landers, California, earthquake of 1992, *J. Geophys. Res.*, *99*, 11,705–11,722.
- Li, X., V. F. Cormier, and M. N. Toksoz (2002), Complex source process of the 17 August 1999 Izmit, Turkey, earthquake, *Bull. Seismol. Soc. Am.*, *92*, 267–277.
- Lienkaemper, J. J., J. S. Galehouse, and R. W. Simpson (1997), Creep response of the Hayward fault to stress changes caused by the Loma Prieta earthquake, *Science*, *276*, 2014–2016.
- Lyakhovskiy, V., Y. Ben-Zion, and A. Agnon (1997), Distributed damage, faulting, and friction, *J. Geophys. Res.*, *102*, 27,635–27,649.
- McClusky, S., et al. (2000), Global Positioning System constraints on plate kinematics and dynamics in the eastern Mediterranean and Caucasus, *J. Geophys. Res.*, *105*, 5695–5720.
- Okada, Y. (1985), Surface deformation due to shear and tensile faults in a half-space, *Bull. Seismol. Soc. Am.*, *75*, 1135–1154.
- Parsons, T., S. Toda, R. S. Stein, A. Barka, and J. H. Dieterich (2000), Heightened odds of large earthquakes near Istanbul: An interaction-based probability calculation, *Science*, *228*, 661–665.
- Peng, Z., and Y. Ben-Zion (2004), Systematic analysis of crustal anisotropy along the Karadere-Düzce branch of the north Anatolian fault, *Geophys. J. Int.*, *159*, 253–274.
- Pestman, B. J., and J. G. Munster (1996), An acoustic emission study of damage development and stress—Memory effects in sandstone, *Int. J. Rock Mech. Min. Sci. Geomech. Abstr.*, *33*, 585–593.
- Reilinger, R. E., et al. (2000), Coseismic and postseismic fault slip for the 17 August 1999 $M = 7.5$, Izmit, Turkey earthquake, *Science*, *289*, 1519–1524.
- Rockwell, T. K., S. Lindval, T. Dawson, R. Langridge, W. Lettis, and Y. Klinger (2002), Lateral offsets on surveyed cultural features resulting from the 1999 Izmit and Düzce earthquakes, Turkey, *Bull. Seismol. Soc. Am.*, *92*, 79–94.
- Saroglu, F., Ö. Emre, and I. Kusçu (1992), *Active Fault Map of Turkey*, General Directorate of Mineral Research and Exploration (MTA), Eskisehir Yolu, 06520, Ankara, Turkey.
- Savage, J. C., and L. M. Hastie (1969), A dislocation model for the Fairview Peak, Nevada, earthquake, *Bull. Seismol. Soc. Am.*, *59*, 1937–1948.
- Sengör, A. M. C., N. Görür, and F. Saroglu (1985), Strike-slip faulting and related basin formation in zones of tectonic escape: Turkey as a case study, in *Strike-Slip Faulting and Basin Formation*, edited by K. T. Biddke and N. Christie-Blick, Spec. Publ. Soc. Econ. Paleont. Miner., Tulsa, *37*, 227–264.
- Simons, M., Y. Fialko, and L. Rivera (2002), Coseismic deformation from the 1999 M_w 7.1 Hector Mine, California, earthquake as inferred from InSAR and GPS observations, *Bull. Seismol. Soc. Am.*, *92*, 1390–1402.
- Stein, R. S., A. Barka, and J. H. Dieterich (1997), Progressive failure on the North Anatolian fault since 1939 by earthquake stress triggering, *Geophys. J. Int.*, *128*, 594–604.
- Straub, C., H. G. Kahle, and C. Schindler (1997), GPS and geologic estimates of the tectonic activity in the Marmara Sea region, NW Anatolia, *J. Geophys. Res.*, *102*, 27,587–27,601.
- Wang, R., F. L. Martin, and F. Roth (2003), Computation of deformation induced by earthquakes in a multi-layered elastic crust—FORTRAN programs EDGRN/EDCMP, *Comput. Geosci.*, *29*, 195–207.
- Wilson, B., T. Dewers, Z. Reches, and J. Brune (2005), Particle size and energetics of gouge from earthquake rupture zones, *Nature*, *434*, 749–752.
- Wright, T., E. Fielding, and B. Parsons (2001), Triggered slip: Observations of the 17 August 1999 Izmit (Turkey) earthquake using radar interferometry, *Geophys. Res. Lett.*, *28*, 1079–1082.

Y. Fialko, Institute of Geophysics and Planetary Physics, Scripps Institution of Oceanography, University of California, San Diego, La Jolla, CA, USA.

Y. Hamiel, Geological Survey of Israel, 30 Malkhe Israel St., 95501 Jerusalem, Israel. (yariv@gsi.gov.il)